Publication Year	2019
Acceptance in OA	2020-07-21T10:12:21Z
Title	Mineralogical analysis of quadrangle Ac-H-10 Rongo on the dwarf planet Ceres
Authors	ZAMBON, Francesca, CARROZZO, FILIPPO GIACOMO, TOSI, Federico, CIARNIELLO, Mauro, Combe, J. Ph., FRIGERI, ALESSANDRO, DE SANCTIS, MARIA CRISTINA, Thangjam, G., Nathues, A., Hoffmann, M., LONGOBARDO, ANDREA, Stephan, K., RAPONI, Andrea, Ammannito, E., Krohn, K., McFadden, L. A., PALOMBA, Ernesto, Raymond, C. A., Russell, C. T., Dawn Science Team
Publisher's version (DOI)	10.1016/j.icarus.2017.09.021
Handle	http://hdl.handle.net/20.500.12386/26546
Journal	ICARUS
Volume	318

Mineralogical Analysis of the Quadrangle Ac-H-10 Rongo on Dwarf Planet Ceres

F. Zambon[a,*], F. G. Carrozzo[a], F. Tosi[a], M. Ciarniello[a], J. Ph. Combe[b], A. Frigeri[a], M.C. De Sanctis[a], G. Thangjam[c], A. Nathues[c], M. Hoffmann[c], A. Longobardo[a], K. Stephan[d], A. Raponi[a], E. Ammannito[e], K. Krohn[d], L.A. McFadden[f], E. Palomba[a], C.A. Raymond[g], C.T. Russell[h], and the *Dawn* Science Team

[a] INAF-IAPS Istituto di Astrofisica e Planetologia Spaziali, Via del Fosso del Cavaliere, 100, I-00133 Rome, Italy;
[b] Bear Fight Institute, 22, Fiddler's Road, P.O. Box 667, Winthrop, WA, 98862, USA;
[c] Max Planck Institute for Solar System Research, Justus-von-Liebig-Weg 3, D-37077 Göttingen, Germany;
[d] Institute of Planetary Research, German Aerospace Center (DLR), Rutherfordstrasse 2, D-12489 Berlin, Germany;
[e] Italian Space Agency (ASI), Via del Politecnico snc, I-00133 Rome, Italy;
[f] NASA/Goddard Space Flight Center, Greenbelt, 8800 Greenbelt Road, MD 20771, USA;
[g] NASA/Jet Propulsion Laboratory and California Institute of Technology, 4800 Oak Grove Drive, Pasadena, CA 91109, USA;
[h] Institute of Geophysics and Planetary Physics, University of California at Los Angeles, 3845 Slichter Hall, 603 Charles E. Young Drive, East, Los Angeles, CA 90095-1567, USA.

Proposed Running Head: Mineralogical Analysis of the Quadrangle Ac-H-10 Rongo on Dwarf Planet Ceres

*** Corresponding author:** Dr. Francesca Zambon
INAF-IAPS Istituto di Astrofisica e Planetologia Spaziali
Via del Fosso del Cavaliere, 100, I-00133 Rome, Italy
Phone: +39-06-45488-760
Email: francesca.zambon@iaps.inaf.it

Version 3.0 (30 April 2017)
To be submitted to:
Icarus
Special issue on the mineralogical mapping of the Ceres quads
(T.B. McCord, F. Zambon, guest editors)

Abstract

Quadrangle Ac-H-10 ‘Rongo’ (22°S-22°N, 288°E-360°E) shows a fairly homogeneous topography, with the presence of some elevations such as *Ahuna Mons*, *Liberalia Mons*, and *Samhain Catenae*. The southern region of the quadrangle is characterized by a lower elevation associated with Urvara and Yalode craters. A substantial variability in the 2.7-μm band depth distribution is observed across the Rongo quadrangle, indicating an east-west gradient in the abundance of Mg-phyllosilicates. The NH_4-phyllosilicates distribution appears quite homogeneous except for some localized regions, such as crater Haulani’s ejecta, the flanks of Ahuna Mons and crater Begbalel. The two band depths at 2.7 and 3.1 μm display an overall low correlation, suggesting a variable degree of mixing between Mg-phyllosilicates and NH_4-phyllosilicates. At the local scale, mineralogical phases other than phyllosilicates are observed. Quadrangle Rongo includes sodium carbonate-rich regions, such as the flanks of Ahuna Mons, a localized area in Liberalia Mons and crater Begbalel, which often display a reduction in both the 2.7- and 3.1-μm band depths, associated with an increased band depth at ~4 μm, related to the presence of Na-rich carbonate phases. This suggests recent hydrothermal activity in this area, due to several episodes of cryovolcanism, or impacts that unveiled a peculiar composition in the shallow subsurface. Alternatively, the crust in this region might show a variable degree of compactness, such that the formation of Na-carbonates is favored only in specific locations (De Sanctis et al., 2016; Ruesch et al., 2016; Zambon et al., 2017). From a geological standpoint, quadrangle Ac-H-10 Rongo shows a correlation between its two main geologic units (Platz et al., 2017) and the distribution of Mg-phyllosilicates, suggesting a link between geology and mineralogy in this area.

1. Introduction

The NASA Dawn mission entered orbit around the dwarf planet Ceres, the largest and most massive object in the main asteroid belt, on 6 March 2015 (Russell et al., 2016). Dawn is equipped with three instruments: the Framing Camera (FC), the Visible and InfraRed Spectrometer (VIR), and the Gamma Ray and Neutron Detector (GRaND) (Sierks et al., 2011; De Sanctis et al., 2011; Prettyman et al., 2011). The broad coverage and variable resolution of the data acquired by Dawn's payload during the overall orbital phase allowed for deciphering the geology, surface composition, mineralogy and internal structure of this intriguing body.

Prior to Dawn, several ground-based observations revealed the presence of an absorption band at ~3 μm. This feature was interpreted as due to structural OH groups and adsorbed or interlayer H_2O molecules in clay minerals, inferring that the dominant minerals on the surface of Ceres were hydrated clay minerals structurally similar to terrestrial montmorillonite (Lebofsky, 1978; Lebofsky et al., 1981). Larson et al. (1979) suggested that the surface of Ceres was compatible with mixtures of opaque materials and hydrated silicates. Other authors suggested that the 3.07 μm band could be due to ammoniated phyllosilicates, specifically ammonium-bearing saponite (King et al., 1992) or hydrated smectite clays (Feierberg et al., 1981). Rivkin et al. (2006) associated the extra absorption near the 3-μm band to Fe-rich cronstedrite and carbonates. The presence of phyllosilicates and carbonate compounds was confirmed by observations carried out with the Keck II telescope (Carry et al., 2008).

Hyperspectral images acquired by VIR at spatial resolution ranging between ~0.10 and ~1.1 km/pixel shed light on Ceres' surface mineralogy. FC data enabled a thorough geologic mapping of the surface, along with high-resolution color mapping complementary to VIR data, and topographic characterization. VIR covers the overall wavelength range between 0.25 and 5.1 μm (De Sanctis et al. 2011), with the goal of identifying the diagnostic signatures of minerals present in its field of view. The thermally corrected average spectrum of Ceres as observed by VIR (Raponi et al., 2017, this issue), reveals the presence of several absorption bands in the spectral range 2.6-4.0 μm (De Sanctis et al., 2015). These spectral signatures are located at 2.72-2.73 μm, 3.05-3.1 μm, 3.3-3.4 μm, and 3.95 μm (ibid). The prominent 2.72-2.73-μm band is diagnostic of hydrous minerals, more specifically Mg-phyllosilicates, the 3.05-3.1-μm band is associated with NH_4-phyllosilicates, and the 3.3-3.4 μm band, which may be typical of organic compounds (Clark 1999, De Sanctis et al., 2017), can also be diagnostic of carbonates when observed in conjunction with the 4 μm band (Milliken and Rivkin, 2009). Hereafter, for simplicity we will refer to the band centered at 2.72 μm as the 2.7 μm band, the band centered at 3.05-3.1 μm band as the 3.1 μm band, the 3.3-3.5 μm band as the 3.4 μm band, and the 3.95 μm band as the 4 μm band. The application of a linear spectral unmixing model to telescopic spectra of Ceres yielded a best fit by using, as spectral end-members, Mg-bearing carbonates such as dolomite, calcite, and brucite (Milliken and Rivkin, 2009). Results of the nonlinear, spectral unmixing model based on the Hapke theory (Hapke, 1981, 1993) indicate that this average spectrum fits quite well with a mixture of NH_4-montmorillonite or NH_4-annite, antigorite, Mg-carbonate, and a spectrally featureless dark component (De Sanctis et al., 2015). On the other hand, spectral mixtures using brucite do not provide good fits. The first spatially resolved map of Ceres obtained on the basis of Dawn optical imagery (Nathues et al., 2015) revealed an overall dark surface (albedo 0.11) (Li et al., 2016) with widespread albedo variations, about 100 high-albedo spots (Palomba et al., 2017, submitted), and the presence of peculiar geological features seen at the local scale (0.01-1km).

Like for Vesta, Ceres' surface has been divided into fifteen quadrangles, which were later named for their respective individual features (Roatsch et al., 2016) (Fig. 1). For each quadrangle, both geologic maps (Williams et al., 2017) and mineralogical maps (Frigeri et al., 2017, this special issue) have been produced. In this paper, similar to what was previously done for the Av-13 Tuccia and Av-14 Urbinia quadrangles on Vesta (Zambon et al., 2015), we discuss the spectral characteristics of the quadrangle

Ac-H-10 Rongo, which is one out of five covering the equatorial region (Lon 288°-360°E, Lat 22°S-22°N) (Fig. 1), bordering Yalode quadrangle in the south (Ammannito et al., 2017, this issue), Occator quadrangle in the weastern side (Longobardo et al., 2017, this issue), Haulani in the eastern side (Tosi et al., 2017, this issue) and Fejokoo quadrangle (Singh et al., 2017, this issue) in the northern side.

2. Data

The orbital mission at Ceres was divided in a number of phases: Survey, High-Altitude Mapping Orbit (HAMO), Low-Altitude Mapping Orbit (LAMO), Extended Low-Altitude Mapping Orbit (E-LAMO), Extended Juling Orbit (E-JO), and Extended Grand Orbit (E-GO). Each phase had a different length and was carried out from a different altitude, with spatial resolution depending on the altitude over the mean surface. In general, the altitude decreased from the Survey to LAMO, and then increased again from the E-LAMO to E-JO and even more from E-JO to E-GO. As a result, in the Survey orbit phase the average pixel resolution was ~1.10 km for VIR and ~0.41 km for FC; from the HAMO orbit it was ~0.38 km for VIR and ~0.14 km for FC; in the LAMO and E-LAMO phases it was ~0.095 km for VIR and ~0.035 km for FC; in the E-JO phase it was ~0.38 for VIR and ~0.14 km for FC (very similar to the resolution achieved in the previous HAMO phase), while in the E-GO phase the spatial resolution of VIR data was relatively coarse, i.e. 1.9-2.0 km/px, and hyperspectral images were acquired only in the spectral subset 0.25-1.0 μm. The most limited spatial coverage and lowest signal-to-noise ratio (SNR) were obtained in LAMO/E-LAMO, which make VIR data acquired in this period less optimal for use and interpretation on a region as broad as an entire quadrangle of Ceres.

The maps shown in this paper were obtained by using VIR data acquired in the Survey and HAMO mission phases, and FC data acquired in HAMO. Prior to mapping, all VIR spectra underwent a series of processings. The data calibration follows the procedure described by Filacchione and Ammannito (2014). Calibrated data were then treated so as to remove instrumental artifacts (Carrozzo et al., 2016) and to remove the thermal emission, which shows up in spectra acquired on the dayside of Ceres at wavelengths longward of ~3.1 µm (Raponi et al. 2017, this issue). A photometric correction based on the Hapke model (Hapke, 1981, 1993; Ciarniello et al., 2017) was applied to thermally corrected data, to normalize to standard observation geometry (solar phase angle $\alpha = 30°$, solar incidence angle $i = 30°$, and emission angle $e = 0°$). Finally, at the end of this post-processing pipeline, global maps of several spectral indices were produced (see Frigeri et al., 2017, this issue).

To complement our analysis, we include also some relevant maps derived by FC data during the HAMO phase. FC has a spatial resolution ~2.67 times better than VIR (Sierks et al. 2011) and obtained a broader coverage than VIR in the HAMO and LAMO/E-LAMO mission stages. FC is equipped with 7 narrow-band filters centered at different wavelengths in the overall spectral range ~0.4-1.0 µm for compositional analysis, and a broadband clear filter meant for geologic analysis (Sierks et al. 2011). In all maps, including the spectral maps described in the previous subsection, longitudes are given in the Ceres coordinate system (Raymond and Roatsch, 2015). A small crater (~0.4 km diameter) named Kait, located in this quadrangle, was chosen by the Dawn Team to define the prime meridian (Roatsch et al., 2016). The location of this small crater is within the envelope of the broad feature identified in Hubble Space Telescope (HST) data to which the previous system (Archinal et al., 2011) was anchored.

3. Tools and techniques

To carry out our mineralogical analysis based on VIR data, we selected the most relevant spectral parameters, i.e. those showing the larger variability. In the following subsections we briefly describe these parameters (see Frigeri et al. 2017, this issue, for more details).

3.1 Framing camera maps

FC data provide a high-resolution context that is useful to complement our mineralogical analysis of

Ceres. In this regard, we selected several FC-derived mosaics: a reflectance mosaic obtained in the clear filter (map scale ~140 m/pixel) (Fig. 2A), a mosaic of spectral slope calculated between 0.555 and 0.829 μm (Fig. 2B), a digital terrain model at a scale of 60 pixels/degree (Fig. 2C), a RGB 'enhanced' color composite mosaic from FC colors: *R*: 0.96 μm; *G*: 0.75 μm; *B*: 0.44 μm (Fig. 2D), a RGB 'Clementine' composite mosaic made from FC color ratios: *R*: 0.75/0.44 μm, *G*: 0.75/0.92 μm, *B*: 0.44/0.75 μm (Fig. 2E), and finally a geologic map that allows us to associate geologic and mineralogical units (Fig. 2F).

The 'Clementine' color composite map (Pieters et al., 1994) is of interest to evaluate local spectral variations at high spatial resolution, which may trace variations in composition. Comparing Clementine color data and VIR spectral maps is indeed a powerful way to highlight possible correlations between mineralogy and spectrally distinct structures seen in color imagery with higher spatial resolution. On the other hand, while the Clementine color code proved to be optimal for lunar and Vesta data, it may not necessarily be the best presentation to trace compositional differences in other rocky bodies of the Solar System. Therefore, to explore the Rongo region we also use a FC enhanced color scheme, to investigate the existence of spectral textures that would otherwise remain elusive or hidden.

3.2 VIR maps

3.2.1 Albedo maps at 1.2 μm and 1.9 μm

The maps shown in Fig. 3 display the albedo obtained by VIR data at two different wavelengths, 1.9 μm (Fig. 3A) and 2.1 μm (Fig. 3B). These wavelengths were chosen so as to avoid spectral regions known or expected to host diagnostic signatures, and are therefore optimal to sample the spectral continuum. As anticipated in Section 2, the albedo was calculated by applying a Hapke photometric correction to the entire dataset (Ciarniello et al., 2017).

3.2.2. Infrared spectral slopes

The spectral slope (Fig. 4) is a useful parameter to investigate surface properties. Spectral slope variations are associated with terrain's maturity and also provide complementary information on the grain size (Clark 1999, Stephan et al., 2017). Lower spectral slope are often associated with young terrains, higher spectral slope values are typical of older terrains (e.g. Nettles et al., 2011, Stephan et al., 2017). Similar to albedo maps computed at 1.2 and 1.9 μm, spectral slope maps were also computed in two distinct regions of the infrared spectrum where no absorption features show up. In particular, we selected two spectral slopes between 1.891-1.163 μm (SI) and 2.250-1.891 (SII). The method used to calculate this parameter is shown in Filacchione et al. 2012, and Frigeri et al. (2017, this issue), describes it in detail.

3.2.3. 2.7 and 3.1 μm band depths

The average reflectance spectrum of Ceres displays a number of absorption bands (De Sanctis et al., 2015). Here we map the depths of the two bands centered at ~2.7 μm and ~3.1 μm (Fig. 5). These bands are associated with magnesium phyllosilcates and ammoniated phyllosilicates, respectively (De Sanctis et al., 2015, Ammannito et al., 2016). The depth of a band gives information about the abundance of the absorbing minerals, but could be also affected by the presence of opaque materials, and the grain size (Clark 1999). Band depth maps are calculated after applying Hapke photometric correction (Ciarniello et al. 2017). For a more detailed description, we refer to Frigeri et al., 2017.

4. Description of the quadrangles

Quadrangle Ac-H-10 Rongo is characterized by numerous impact craters in the broad diameter range <100 m to 205 km and variable states of preservation-from fresh to highly degraded. A number of gently rising and partially coalesced landforms are observed across the quadrangle (Platz et al., 2017).

The FC-derived reflectance map obtained in HAMO (Fig. 2A) reveals the presence of several features: *Ahuna Mons* (Lat 10.48°S, Lon 316.2°E, diameter ~20km) and *Liberalia Mons* (Lat 6.2°N, Lon 311.01°E, diameter ~90 km), *Samhain* and *Uhola* catenae in the western part of the quadrangle, and several impact craters. Those with an official designation by the IAU and diameters in the range 40-100 km are: *Begbalel* (Lat 17.7°N, Lon 325.35°E, diameter ~102 km), *Rongo* (Lat 21.3°N, Lon 348.71°E, diameter 68 km), with several crater wall collapse events as evidenced by the pronounced scalloped rim (Platz et al., 2017), which gives the name to the quadrangle, and *Hatipowa* (Lat 16.8°S, Lon 357.71°E, diameter 40 km). The maximum topographic relief across the quadrangle is ~11.1 km (Fig. 2C) (Platz et al., 2017). The main feature of this quadrangle, Ahuna Mons, with a local radius of 485 km (19.4 km × 13.8 km, and a maximum height of ~5 km o its steepest side), is the highest elevation in this quadrangle and the highest mountain on Ceres (ibid.). Ahuna Mons' flanks are smooth and are composed of bright material, primarily salts and carbonates (Ruesch et al., 2016, Zambon et al., 2017a). The contact to the surrounding cratered terrain is sharp and only gradational where flank-induced flow deposition occurred. The summit region exhibits linear to arcuate ridges with no preferred orientation (Platz et al., 2017). Other elevations in this quadrangle are Liberalia Mons, Kait crater's area, and Samhain Catenae. Conversely, the deepest topography is observed in the southern part of the quadrangle (local radius 417 km), in Yalode basins (Ammannito et al., 2017, this issue).

The geologic map (Fig. 2F) highlighted two broad geological units: the most widespread is cratered terrain, which covers large part of the quadrangle and more generally is the dominant surface unit on Ceres, and Yalode ejecta material in the southwestern part of the quadrangle. With respect to these two broad units, younger geologic units are found at the local scale: tholus material matching Ahuna and Liberalia Mons, bright crater material in Begbalel, Liberalia Mons and other two features in the north-eastern part of the quadrangle (Fig. 2F). Hummocky crater floor material is present inside many craters, such as Begbalel, Rongo and Hitipowa. Haulani crater's ejecta, coming from the nearby Ac-H-6

Haulani quadrangle, have been identified as a separate, crater ray material unit. Individual ejecta rays can be traced for up to 450 km (Platz et al., 2017). The southwestern part of the quadrangle, including Samhain and Uhola catenae, is dominated by rough-textured material interpreted to represent ejecta from Yalode Crater (260 km in diameter). Yalode ejecta material is often dissected and is clearly distinct in texture from the cratered terrain. Detailed analysis of crater size-frequency distributions revealed model ages, for the two main geological units, of about 540 Ma Yalode crater and about 1.8 Ga as formation age for the cratered terrain. Cratered terrain exhibits large variations in crater densities across the globe (Hiesinger et al., 2016) with resulting model ages ranging between 1.4-3.4 Ga (Pasckert et al., 2017, Williams et al., 2017, see also Platz et al., 2017).

5. Global mineralogy of Ac-H-10 Rongo

The enhanced color composite mosaic (red: 0.96 μm; green: 0.75 μm; blue: 0.44 μm) (Fig. 2D) highlights that most of the surface in quadrangle Ac-H-10 (and more generally on Ceres) displays a brownish background color, punctuated by other units characterized by different colors. Haulani crater's ejecta, which dominate the eastern side of the quadrangle, is one the most prominent multispectral unit, characterized by a striking bluish color (Tosi et al., 2017, this issue). Similar to Haulani's ejecta, the flanks of Ahuna Mons and crater Begbalel are also characterized by a bluish color shade. The same color dominates the western side of the quadragle, bordering the Occator quadrangle (Longobardo et al., this issue) in correspondence with Samhain Catenae, while Liberalia Mons is stands out for its albedo (0.037 ± 0.002 at 1.2 μm, 0.039 ± 0.001 at 1.9 μm). In the Clementine color presentation (red: 0.75/0.44 μm, green: 0.75/0.92 μm, blue: 0.44/0.75 μm), dark materials appear dark bluish/violet, and bright materials are yellow-green, with intermediate albedo surfaces appearing cyan (Fig. 2E). The Clementine composite map of quadrangle Ac-H-10 shows that most of the surface is reddish, while Haulani craters' ejecta, the bright area in Liberalia Mons, crater Begbalel and the region of Samhain Catenae (Fig. 2D) stand out in displaying an overall bluish/violet color. Ahuna Mons is the only feature of this quadrangle showing a cyan color around the flanks. The map of spectral slope, calculated between 0.555 and 0.829 μm (Fig. 2B), reveals that the majority of the quadrangle has a greenish to whitish color, indicating a null (flat) or slightly positive slope value. Haulani ejecta stands out for its magenta and violet colors corresponding to negative values of spectral slope (Stephan et al., 2017). Along with Haulani ejecta, also the flanks of Ahuna Mons and Liberalia Mons are characterized by negative spectral slopes. Extreme negative values (down to -0.148) are recorded in Ahuna Mons and Liberalia Mons. On a broader scale within quadrangle Ac-H-10, the 0.555-0.829 μm spectral slope does not show any particular trend. Age determination indicates that the bluish material seen in Figs, 2D and 2E is mainly associated with the youngest impact craters or cryovolcanic events on Ceres (Nathues et al., 2016; Schmedemann et al., 2016). The spectral slope (SI and SII) maps derived by VIR in the near infrared range, show similar results. SI covers a range of values between 0.05 and 0.14, while SII spans from -0.03 and 0.07, with an average value of 0.095 ± 0.014 for SI, and 0.022 ± 0.015 for SII. The region showing the largest variability in terms of spectral slopes is the flanks of Ahuna Mons, in which both SI and SII show the lowest values (slope I: 0.05, slope II -0.03) within the quadrangle. Along with Ahuna flanks, Liberalia Mons and Haulani ejecta (Tosi et al., 2017, this issue) also display low infrared spectral slope values. The rest of the quadrangle is characterized by flat or slightly positive spectral slope values. The blue slope is generally a proxy for younger, less processed material. This implies that Ahuna Mons and Haulani's ejecta are also the youngest features on Ceres (Ruesch et al. 2016; Stephan et al 2017; Schroeder et al, 2017).

From the FC-derived clear filter reflectance mosaic (Fig. 2A), whose reflectance values range from 0.01 to 0.06, one can infer the existence of bright and dark materials, which stand out as having substantially higher or lower reflectances than the quadrangle's average value of 0.03.

Albedo maps retrieved in the near infrared on the basis of VIR data (Fig. 3) at 1.2 and 1.9 μm show a fairly homogeneous trend with an average albedo of 0.034 ± 0.001 at 1.2 μm and 0.036 ± 0.001 at 1.9 μm. Nevertheless, some regions, such as the flanks of Ahuna Mons (0.038 ± 0.001) (Ruesch et al., 2016; Zambon et al. 2017), and a localized area in Liberalia Mons (0.037 ± 0.002 at 1.2 μm, 0.039 ± 0.001 at 1.9 μm), apper brighter than the average, while Haulani's ejecta are darker (0.0335 ± 0.0006 at 1.2 μm and 0.0356 ± 0.0006 at 1.9 μm) (Stephan et al., 2017; Krohn et al., 2017; Tosi et al., 2017, this issue), as much as Ahuna Mons' top (0.0313 ± 0.0008 at 1.2 μm and 0.0331 ± 0.0008 at 1.9 μm). The analysis of the strongest bands of Ceres spectra, those at 2.7 μm and 3.1 μm interpreted as due to Mg- and NH_4-rich phyllosilicates, do not emphasize any band center variation, implying no relevant compositional changes. Conversely, band depth maps (Fig. 5) reveal a regional variability within the quadrangle. 2.7 μm band depth values span between 0.186 and 0.212, while the band depth at 3.1 μm ranges between 0.07 and 0.1. The eastern region of the Rongo quadrangle is depleted in Mg-phyllosilicates with respect to the western part (Fig 5A). The region between longitude 336°-348°E and latitude 22°S-10°N in latitude presents the highest 2.7 μm band depth values within this quadrangle (0.212), while the lowest values are registered in the Ahuna Mons flanks (0.186). The 3.1 μm band depth (Fig. 5B) shows a homogeneous distribution, with a lower amount of NH_4-phyllosilicates, mostly corresponding to the flanks of Ahuna Mons flanks and Haulani's ejecta, but also in the region of Samhain catenae and crater Bagbalel.

In Fig. 6, we show maps that correlate the 2.7 μm band with the 3.1 μm band. Red-green-blue color composites are commonly used to represent three different datasets; however the drawback is that it is not possible to represent all the colors of the map in a single color table (a real one would have three dimensions), which limits the accuracy and relevance of the interpretations. It is however possible to represent two parameters using two-dimensional color tables based on mixtures of four or more colors (e.g. Combe et al., 2015; Combe et al., 2017, this issue). The interpretation of the colors can be eased by displaying a two-dimensional scatterplot of the dataset at the same scale or as an overlay to the color table. Fig. 6A is produced by combining FC albedo map and using VIR data with the following color combination: red = 2.7 μm band depth, green = FC albedo at 0.45 μm, blue = 3.1 μm band depth. In this color code, green areas have a high albedo, while redder areas have higher 2.7 μm band depth, and bluer areas have higher 3.1 μm band depth. The areas where all three are present in high amount appears white. In Fig. 6B, same global and Ac-H-10 quadrangle map is shown using a color scale which emphasizes only extremes spectral composition. The colors represented in panel c have a direct correspondence to the colors on the map (Fig. 6) (see Combe et al., 2017, this issue and Singh et al., 2017, this issue).

The yellow region between Samhain catenae and Liberalia Mons (Fig. 6A) shows low average values for both the band depths, while the regions in blue, which mostly mark the northern and the southeastern region of the quadrangle, present the highest values for both the band depths. The yellow region in the eastern region of the quadrangle corresponds to the Haulani's ejecta. However, the flanks of Ahuna Mons display the minimum values for both the band depths. Ahuna Mons is a recent feature, younger than the neighboring crater. The features showing the larger difference in terms of band depth (Fig. 6B) are Ahuna Mons and Haulani ejecta.

The Rongo quadrangle is characterized by significant spectral variability on the basis of VIR-derived spectral parameters and data, which in turn indicate substantial mineralogical variations. Ac-H-10 is generally dominated by a widespread spectral unit, on which other smaller and younger units are superimposed. For example, the geologic unit classified as Yalode ejecta material in the southeastern region of the quadrangle seems to be characterized by lower values of the 2.7 μm band depth, while the widespread unit named cratered terrain is characterized by the highest values of the 2.7 μm band depth. The unit classified as tholus material, which includes both Ahuna Mons and Liberalia Mons, seems to be characterized by higher albedo and medium-to-low values of the two band depths for Ahuna Mons, while higher 3.1 μm band depths values are found for Liberalia Mons.

The smooth unit and the 17-km crater unit close to Ahuna have a similar age: 210 ± 30 Ma and 160 ± 30 Ma, respectively, using the Lunar Derived Model or 70 ± 20 Ma and 70 ± 20 Ma, respectively, using the Asteroid Derived Model (Ruesch et al., 2016). Low spectral slope values confirm the younger age of this structure. Ahuna Mons has been interpreted as an extrusion due to several episodes of cryovolcanism. The composition of its flanks highlight Na-rich carbonate material coming from the subsurface (Zambon et al., 2017).

The histogram in Fig. 7A, related to the frequency of the band depths at 2.7 μm and 3.1 μm, shows that ~70% of 3.1 μm band depth values within the quadrangle range between 0.08 and 0.9, while most 2.7 μm band depth values span around 0.19 and 0.21. Consistent with the average reflectance spectrum of the surface of Ceres as measured by VIR, where the absorption centered at 2.72-2.73 μm is broader than the absorption centered at 3.05-3.1 μm (De Sanctis et al., 2015), the 2.7-μm band depth is larger than the 3.1 μm band depth, with most recurrent values in the range 0.188-0.212 (average value 0.199) for 2.7 μm band depth and 0.069-0.1 (average value 0.084) for the 3.1 μm band. The 3.1 μm distributions have a narrow width, with balanced maximum values of frequency and comparable shapes hardly modeled by a Gaussian fit, which overall demostrates the goodness of photometric correction, and at the same time testifies a relatively homogeneous distribution of the abundance of the featureless spectral endmember across the entire quadrangle. However, the 2.7 μm band depth distribution is narrower than the 3.1 μm distribution, indicating a higher degree of variability in the abundance of ammoniated phyllosilicates across the quadrangle, as shown in Fig. 5B. For comparison, in other nearby quadrangles of Ceres the observed statistics may show a slightly different distribution (e.g., Tosi et al., 2017, this issue). This aspect is also important to associate the values of 2.7 and 3.1 μm band depth that we observe to relative abundances of Mg-rich and NH_4-rich phyllosilicates, respectively.

The band depth value, which is indicative of a mineral's abundance, may also be affected by the presence of opaque phases and by the grain size (Clark, 1999). In order to quantify abundance values, a spectral unmixing model has to be applied to the observed spectral data, which is beyond the scope of our work. However, from the spectral unmixing modeling carried out previously to establish the global average mineralogy of Ceres, it turns out that best fits with respect to the average reflectance spectrum of Ceres as measured by VIR are obtained by using antigorite with a grain size of 90 μm, Mg-carbonates with a grain size of 10 μm, and a featureless dark component with a grain size of 80 μm (the grain size for NH_4-rich phyllosilicates could not be determined unequivocally) (Fig. 4a and Extended Data Table 2 in De Sanctis et al., 2015). So, under the reasonable assumption that these grain size values are recurrent on a broadly regional scale including quadrangle Ac-H-10, our 2.7 and 3.1 μm band depth values may be associated to mineral abundances rather than to variations in the grain size distribution.

The density scatterplot in Fig. 7B does not show any significant correlation between the two bands. The linear model proves inadequate to describe the trend of the ratio of Mg-rich/NH_4-rich phyllosilicates: as revealed by the chi-square, the distribution is essentially non-linear, and the average coefficient of determination is low, meaning that a substantial correlation between these two variables is generally not met throughout the quadrangle, but only for specific geologic features found at the local scale.

By mapping the value of the ratio between the measured 2.7 μm band depth and the 2.7 μm/3.1 μm band depth linear approximation (Fig. 8), one can see that the northeastern part of the quadrangle, in green, is the closest to the linear model, while the southwestern region presents lower values with respect to the linear model and the blue region indicates an opposite behavior. Locations with 2.7 μm band depth values significantly lower than the linear model displayed in Fig. 8, i.e. with a lower value of the ratio Mg-rich/NH_4-rich phyllosilicates, generally correspond to the area of Ahuna Mons and Yalode ejecta material. Conversely, values significantly higher than the linear model, i.e. with a higher value of the ratio Mg-rich/NH_4-rich phyllosilicates, concentrate in the southeastern part of the quadrangle.

Other than the 2.7 and 3.1 μm absorption bands, also other two prominent band at 3.3-3.5 μm and 3.94-4.0 μm have been observed on the basis of VIR data (De Sanctis et al., 2015). When observed together, the 3.4 μm band and the 4 μm bands are indicative of the presence of carbonates (De Sanctis et al., 2015; Carrozzo et al., 2017, submitted). Conversely, the existence of the 3.4 μm band alone is indicative of organic compounds, as recentely discovered in the area of crater Ernutet in Ac-H-2 Coniraya quadrangle (Raponi et al., 2017, this issue) by De Sanctis et al. (2017).

Non-linear spectral unmixing based on the Hapke method indicates that the surface of Ceres is characterized by an overall distribution of (Mg, Ca)-carbonates, with localized areas enriched in Na-carbonates, such as crater Occator (De Sanctis et al., 2016), Azzaca area (Carrozzo et al., 2017, this issue), crater Kupalo (De Sanctis et al., 2017, this issue) and the flanks of Ahuna Mons (Zambon et al., 2016). As shown by Carrozzo et al. (2017, submitted), also Ac-H-10 Rongo includes more than one Na-rich site: besides Ahuna Mons, Na-rich carbonates have been found in Liberalia Mons, in crater Begbalel, and in crater Hatipowa. Na-rich carbonates are believed to be related to past hydrothermal activity, brought out by impacts or cryovolcanism episodes.

5. Discussion and Conclusion

A thorough mineralogical analysis of the Ac-H-10 Rongo quadrangle, based on the interpretation of several spectral parameters, indicates a variegated mineralogy. Rongo’s topography includes high elevations such as Ahuna Mons and Liberalia Mons, and depressed regions such as the area of craters Urvara and Yalode and the region east of crater Begbalel. From a mineralogical standpoint, we can identify different units. The parameters that show larger variability are the 2.7 and 3.1 μm band depths, which highlight a trend in the distribution of the Mg-and and NH_4-phyllosilicates, respectively. The band depth at 2.7 μm presents larger values in the eastern region of the quadrangle, matching the oldest geologic unit, i.e. cratered material. The southwestern region of the quadrangle, corresponding to Yalode ejecta material, is characterized by a depletion in OH-rich minerals, as much as the ejecta of crater Haulani. The band depth distribution at 3.1 μm appears more homogeneous, but a depletion in NH_4-phyllosilicates is observed in Haulani's ejecta. In general, the two band depths are mostly uncorrelated.

The main tholus within quadrangle Ac-H-10 Rongo is Ahuna Mons, a young feature interpreted as extrusion due to multiple episodes of cryovolcanism (Ruesch et al., 2016). Ahuna Mons was formed by a volcanic process involving the ascent of cryomagma and extrusion onto the surface followed by dome development. The mons and tholus upon which it sits might have shared a common reservoir at depth (Ruesch et al., 2016). Their different morphologies might be related to a change in the rheological properties (e.g., chemistry and temperature) of the reservoir with time or during ascent (ibid.). This is confirmed by a generally greater abundance of Na-carbonates in Ahuna compared to the surroundings. Although the overall composition is not too dissimilar to what is found elsewhere on Ceres, at the local scale Ahuna Mons emerges to have a lower abundance of ammoniated and hydrous mineral phases, a reduction of the spectral slope both in the visible and in the infrared range, and a greater abundance of Na-rich carbonates than the surrounding areas observed at the same spatial resolution (Platz et al., 2017; Zambon et al., 2017). The presence of Na-carbonates has been interpreted as evidence of recent hydrothermal activity (De Sanctis et al., 2016) and is consistent with a cryovolcanic origin of Ahuna Mons, which would locally raise a portion of terrain by exposing fresh subsurface material richer in carbonates. Besides Ahuna Mons, also other region in Rongo quadrangle display Na-carbonates enrichments. A further ancient tholus located within crater Begbalel is also interpreted to be a cryovolcanic edifice by Platz et al. (2017), and also here Na-carbonates have been observed (Carrozzo et al., 2017). Also a third tholus, Liberalia Mons, displays Na-carbonates deposits, in correspondence with a small bright crater on the top. Other tholi are also identified in quadrangle Ac-H-5 Fejokoo (Singh et al., 2017, this issue). Haulani crater's ejecta material displaying a substantial negative spectral slope is the product of material melted and vaporized during the impact event, which may have been ejected to significant distances at high velocities (Stephan et al., 2017). The composition we observe today in Haulani's ejecta may have been favored by both the pre-existing mineralogy and the characteristics of the impact event. Space weathering, in terms of diurnal temperature variations and micrometeoritic impacts forming a regolith layer of fine-grained phyllosilicate dust, may be responsible for the fading of the blue color over time (Stephan et al., 2017). Ahuna Mons is among the bluest units on Ceres, after crater Haulani and crater Oxo (Singh et al., 2017, this issue), which is indicative of a younger age and less processed material.

In general, in correspondence with Na-carbonates enrichment, we observe an abundance reduction of Mg- and NH_4-phyllosilicates. Na-carbonates are endogenous on Ceres and this material is typical of the underlying layers of the surface, deposited after brine evaporation related to hydrothermal activities, brought out by impact or episodes of cryovolcanism (De Sanctis et al., 2016, Ruesch et al., 2016). Ceres surface is highly cratered (Williams et al., 2017), but Na-carbonates are present only in some specific regions seen at the local scale, indicating a non-uniform distribution of this compound on Ceres' shallow subsurface or alternatively a different compactness of the crust at different locations. Furthermore, the depletion in Mg-phyllosicates observed in specific regions could be related to the energy of impact, which may have caused a loss of OH-rich minerals but not of NH_4-phyllosilicates, explaining the overall non-correlation between this two bands' strength. Our analysis shows that quadrangle Ac-H-10 Rongo has a variegated mineralogy, which is indicative of a recent past activity. Furthermore, a link between the two main geological units and spectral variability is been observed.

Future work should focus on VIR data obtained in the main areas of Rongo quadrangle at the highest available pixel resolution (i.e., ~0.10 km), applying spectral unmixing techniques (e.g., Zambon et al., 2016; Tosi et al., 2015) able to quantify the abundances of a number of mineral species known or expected to exist at the surface, including carbonates.

Acknowledgments

We thank the Italian Space Agency (ASI) and NASA for supporting this work. The VIR instrument was funded and coordinated by the ASI and built by Selex ES, with the scientific leadership of the Institute for Space Astrophysics and Planetology, Italian National Institute for Astrophysics, Italy. The VIR is operated by the Institute for Space Astrophysics and Planetology, Rome, Italy. A portion of this work was carried out at the Jet Propulsion Laboratory, California Institute of Technology, under contract to NASA. Dawn data are archived in NASA's Planetary Data System; VIR spectral data may be obtained at https://sbn.psi.edu/pds/resource/dwncvir.html

Figure captions

Figure 1: Index map of the fifteen quadrangles that are defined for the surface of Ceres (Roatsch et al., 2016). The quadrangle images are made using HAMO Framing Camera clear filter images of Ceres, obtained by the Framing Camera team at the Max Planck Institute and German Aerospace Center (DLR). Red rectangle indicates the quadrangle Ac-H-10 Rongo, located at 288°- 360°E, 22°S - 22°N.

Figure 2: Maps of Ac-H-10 Rongo quadrangle retreived by the Framing Camera (FC) data relative to the HAMO phase of the mission (spatial resolution ~ 140 m/px). **A:** Reflectance map of Ac-H-10 Rongo, obtained through photometric correction of FC clear-filter data acquired in the HAMO mission phase. Surface features that have received an official designation by the IAU are marked in yellow color. **B:** RGB composite of the Ac-H-10 Rongo quadrangle showing spectral slope calculated between 0.555 and 0.829 μm. **C:** Topography/elevation map of Rongo quadrangle derived using HAMO DTM (Preusker et al., 2016), at a scale of 60 pixels/degree. The rainbow color palette follows topography (local radius), with the highest elevations in red and the lowest terrains in dark blue/violet.
D: RGB composite of the Ac-H-10 Rongo quadrangle made from FC colors: *R*: 0.96 μm; *G*: 0.75 μm; *B*: 0.44 μm ('enhanced' color composite). Compared to the Clementine presentation, this color scheme enhances differences in albedo. **E:** RGB composite of the Ac-H-10 Rongo quadrangle made from FC color ratios: *R*: 0.75/0.43 μm, *G*: 0.75/0.92 μm, *B*: 0.43/0.75 μm ('Clementine' color composite). Color ratios may enhance differences in material and composition. **F:** Geologic map of Ac-H-10 Rongo, adapted from Platz et al. (2017). The broad brownish geologic unit is mapped as 'cratered terrain' (*crt*), while the pink color indicates 'Yalode ejecta' (*Ye*). Red patches of 'tholus material' (th) are found in the correspondece with Ahuna Mons and in the vicinity of Begbalel crater. Light yellow patches are 'crater bright material' (*cb*), while yellow patch represent 'crater material' (*c*). Light pink and dark green indicate 'crater floor material hummocky' (*cfh*) and 'talus material' (*ta*), respectively.

Figure 3: A: Reflectance map of Ac-H-10 Rongo, obtained through photometric correction of VIR data acquired at 1.2 μm in the Survey and HAMO mission phases, interpolated on a grid with a fixed resolution of ~140 m/pixel, photometrically corrected by using the method described by Ciarniello et al. (2017), i.e. a Hapke photometric correction to standard observation geometry (i=30°, e=0°, α=30°). **B:** Reflectance map of Ac-H-10 Rongo, obtained through photometric correction of VIR data acquired at 1.9 μm in the Survey and HAMO mission phases, interpolated on a grid with a fixed resolution of 140 m/pixel. The same photometric correction of Panel A was applied.

Figure 4: Two spectral slopes, calculated in the near infrared range 1.163-1.891 μm (**A**) and 1.891-2.250 μm (**B**) on the basis of VIR infrared data. These spectral slopes are essentially consistent with the spectral slope obtained from FC data in the visual range 0.555-0.829 μm at higher spatial resolution (Fig. 2B): i.e., it is confirmed that crater Haulani ejecta, Ahuna Mons flanks and a localized region in Liberealia Mons generally corresponds to a neat reduction in spectral slopes.

Figure 5: Distribution of 2.7 μm band depth (**A**) and 3.1 μm band depth (**B**) values across the Rongo quadrangle, derived from VIR data. These band depths are sensitive to the abundance of magnesium-bearing phyllosilicates and ammoniated phyllosilicates, respectively, and to the presence of opaque contaminants. The overall distribution spans from lower depth (dark blue to blue) to greater depth (red to dark red). Ahuna Mons flanks and Haulani ejecta are associated with the spectrally distinct material have shallower 2.7 and 3.1 μm band depth values.

Figure 6: **a:** 2D scatterplot of 2.7 μm band depth as a function of 3.1 μm band depth computed for the entire surface of Ceres. **b:** four-color key and legend for Panel c (this figure) and panel A and B. Materials depleted in both Mg-rich phyllosilicates and NH4-rich phyllosilicates appear in yellow-orange colors, while materials enriched in both Mg-rich phyllosilicates and NH4-rich phyllosilicates are displayed in blue. The green color marks materials with enhanced abundance of Mg-rich phyllosilicates and depletion of NH_4-rich phyllosilicates, while the purple color highlights an opposite situation, i.e. materials depleted in Mg-rich phyllosilicates and a relatively high abundance of NH_4-rich phyllosilicates. **c:** Same 2D scatterplot of (a) superimposed on the four-color scheme represented in (b). **A:** four-color map of correlation between 2.7 μm band depth and 3.1 μm band depth. In this map, all VIR pixels are represented by a color according to the scheme defined panel b. **B:** Same kind of map as (A), but in this case the four-color map is partially masked by the 2D-scatter plot from the global dataset represented in panel a. In this map, only the purest compositions are represented by colored pixels, while all the others are dark.

Figure 7: **A:** Histograms of 2.7 μm band depth and 3.1 μm band depth values measured across quadrangle Ac-H-10 (after photometric correction), displayed in dark gray and light gray colors, respectively. A Gaussian fit is superimposed in the light blue color. The most recurrent values are in the range 0.19-0.22 (average value 0.195) for 2.7 μm band depth and 0.08-0.09 (average value 0.085) for 3.1 μm band depth. **B:** Density scatterplot of 2.7-μm band depth as a function of 3.1-μm band depth computed for the quadrangle Ac-H-10. A linear fit model (white dashed line) is superimposed on the distribution. Most data concentrate around the average values. The cluster shows a large spread and a moderate-to-low correlation in the linear fit model

Figure 8: Ratio between the measured 2.7 μm band depth and the 2.7 μm band depth /3.1 μm band depth linear fit model. This map shows where the surface material departs from an ideally linear correlation between the abundance of the two major mineral species. Dark blue to blue colors mark locations that have shallower 2.7 μm band depth than the linear model, while red to dark red shades mark locations that have larger 2.7 μm band depth than the linear model. If 2.7 μm band depth was perfectly correlated with 3.1 μm band depth, this map would appear uniformly green.

References

Ammanito, E., et. al., 2017. Icarus this issue.

Ammannito, E., DeSanctis, M. C., Ciarniello, M., Frigeri, A., Carrozzo, F. G., Combe, J.-P., Ehlmann, B. L., Marchi, S., McSween, H. Y., Raponi, A., Toplis, M. J., Tosi, F., Castillo-Rogez, J. C., Capaccioni, F., Capria, M. T., Fonte, S., Giardino, M., Jaumann, R., Longobardo, A., Joy, S. P., Magni, G., McCord, T. B., McFadden, L. A., Palomba, E., Pieters, C. M., Polanskey, C. A., Rayman, M. D., Raymond, C. A., Schenk, P. M., Zambon, F., Russell, C. T., Sep. 2016. Distribution of phyllosilicates on the surface of Ceres. Science 353, aaf4279.

Archinal, B. A., A'Hearn, M. F., Bowell, E., Conrad, A., Consolmagno, G. J., Courtin, R., Fukushima, T., Hestroffer, D., Hilton, J. L., Krasinsky, G. A., Neumann, G., Oberst, J., Seidelmann, P. K., Stooke, P., Tholen, D. J., Thomas, P. C., Williams, I. P., Feb. 2011. Report of the IAU Working Group on Cartographic Coordinates and Rotational Elements: 2009. Celestial Mechanics and Dynamical Astronomy 109, 101–135.

Carrozzo, F. G., De Sanctis, M. C., Raponi, A., Ammanito, E., Castillo- Rogez, J. C., Ehlmann, B. L., Marchi, S., Stein, N., Ciarniello, M., Tosi, F., Capaccioni, F., Capria, M. T., Fonte, S., Formisano, M., Frigeri, A., Giardino, M., Longobardo, A., Magni, G., Palomba, E., Zambon, F., Raymond, C. A., Russel, C. T., 2017. Nature, formation and distribution of Carbonates on Ceres . In preparation.

Carrozzo, F. G., et. al., 2017. The Mineralogy of the Nawish Quadrangle of Ceres. Icarus, this issue.

Carry, B., Dumas, C., Fulchignoni, M., Merline, W. J., Berthier, J., Hestrof- fer, D., Fusco, T., Tamblyn, P., 2008. Near-infrared mapping and physical properties of the dwarf-planet Ceres. Astronomy and Astrophysics 478 (1), 235–244. DOI: 10.1051/0004–6361:20078166.

Ciarniello, M., De Sanctis, M. C., Ammannito, E., Raponi, A., Longobardo, A., Palomba, E., Carrozzo, F. G., Tosi, F., Li, J.-Y., Schroeder, S. E., Zambon, F., Frigeri, A., Fonte, S., Giardino, M., Pieters, C. M., Ray- mond, C. A., Russell, C. T., Feb. 2017. Spectrophotometric properties of dwarf planet Ceres from the VIR spectrometer on board the Dawn mission. 598, A130.

Clark, R. N., 1999. Remote Sensing for the Earth Sciences - Manual of Re- mote Sensing. Vol. 3. John Wiley and Sons, New York.

Combe, J.-P., et. al., 2017a. The Surface Composition of Ceres Ezinu quad- rangle analyzed by the Dawn mission. Icarus, this issue.

Combe, J.-P., et. al., 2017b. Exposed H2O- rich areas detected on Ceres with the Dawn Visible and InfraRed mapping spectrometer. Icarus, this issue.

Combe, J.-P., McCord, T. B., De Sanctis, M. C., Ammannito, E., Raymond, C. A., Russell, C.T., 2015. Reflectance and hydrated materials of Vesta. Icarus.

De Sanctis, M., Coradini, A., Ammannito, E., Filacchione, G., Capria, M., Fonte, S., Magni, G., Barbis, A., Bini, A., Dami, M., Ficai-Veltroni, I., Preti, G., the VIR Team, 2011. The VIR Spectrometer. Space Science Reviews 163, 329–369. DOI: 10.1007/s11214–010–9668–5.

De Sanctis, M. C., Ammannito, E., McSween, H. Y., Raponi, A., Marchi, S., Capaccioni, F., Capria, M. T., Carrozzo, F. G., Ciarniello, M., Fonte, S., Formisano, M., Frigeri, A., Giardino, M., Longobardo, A., Magni, G., McFadden, L. A., Palomba, E., Pieters, C. M., Tosi, F., Zambon, F., Raymond, C. A., Russell, C. T., Feb. 2017. Localized aliphatic organic material on the surface of Ceres. Science 355, 719–722.

De Sanctis, M. C., Ammannito, E., Raponi, A., Marchi, S., McCord, T. B., McSween, H. Y., Capaccioni, F., Capria, M. T., Carrozzo, F. G., Cia- rniello, M., Longobardo, A., Tosi, F., Fonte, S., Formisano, M., Frigeri, A., Giardino, M., Magni, G., Palomba, E., Turrini, D., Zambon, F., Combe, J.-P., Feldman, W. C., Jaumann, R., McFadden, L. A., Pieters, C. M., Prettyman, T. H., Toplis, M. J., Raymond, C. A., Russell, C. T., 2015. Ammoniated phyllosilicates with a likely outer Solar System origin on (1) Ceres. Nature 528 (7581), 241–244. DOI: 10.1038/nature16172.

De Sanctis, M. C., et. al., 2017. Ac-H-11 Sintana and Ac-H-12 Toharu quad- rangles: Assessing the large and small scale heterogeneities of Ceres' sur- face. Icarus, this issue.

De Sanctis, M. C., Raponi, A., Ammannito, E., Ciarniello, M., Toplis, M. J., McSween, H. Y., Castillo-Rogez, J., Ehlmann, B. L., Carrozzo, F. G., Marchi, S., Zambon, F., Capaccioni, F., Capria, M. T., Fonte, S., Formisano, M., Frigeri, A., Giardino, M., Longobardo, A., Magni, G., Palomba, E., McFadden, L. A., Pieters, C. M., Jaumann, R., Schenk, P. M., Mugnolo, R., Raymond, C. A., Russell, C. T., 2016. Bright carbon- ate deposits as evidence of aqueous alteration on Ceres. Nature In press, DOI: 10.1038/nature18290.

Feierberg, M. A., Lebofsky, L. A., Larson, H. P., 1981. Spectroscopic evidence for aqueous alteration products on the surfaces of low-albedo aster- oids. Geochimica et Cosmochimica Acta 45, 971–981. DOI: 10.1016/0016– 7037(81)90121–6.

Filacchione, G., Capaccioni, F., Ciarniello, M., Clark, R. N., Cuzzi, J. N., Nicholson, P. D., Cruikshank, D. P., Hedman, M. M., Buratti, B. J., Lunine, J. I., Soderblom, L. A., Tosi, F., Cerroni, P., Brown, R. H., McCord, T. B., Jaumann, R., Stephan, K., Baines, K. H., Flamini, E., 2012. Saturn's icy satellites and rings investigated by Cassini– VIMS: III – Radial compositional variability. Icarus 320, 1064–1096. DOI: 10.1016/j.icarus.2012.06.040.

Filacchione, G., and Ammannito, E., 2014. DAWN VIR CALIBRATION DOCUMENT. Version 2.4, http://sbn.psi.edu/archive/dawn/vir/DWNVVIR_I1B/DOCUMENT/VIR_CALIBRATION/VIR_CALIBRATION_V2_4.PDF.

Frigeri, A., et. al., 2017. The spectral parameter maps of Ceres from NASA-DAWN VIR data. Icarus, this issue.

Hapke, B., 1981. Bidirectional reflectance spectroscopy. I - Theory. Journal of Geophysical Research 86, 3039–3054. DOI: 10.1029/JB086iB04p03039.

Hapke, B., 1993. Theory of Reflectance and Emittance Spectroscopy.

Hiesinger, H., Marchi, S., Schmedemann, N., Schenk, P., Pasckert, J. H., Neesemann, A., O'Brien, D.

P., Kneissl, T., Ermakov, A. I., Fu, R. R., Bland, M. T., Nathues, A., Platz, T., Williams, D. A., Jaumann, R., Castillo-Rogez, J. C., Ruesch, O., Schmidt, B., Park, R. S., Preusker, F., Buczkowski, D. L., Russell, C. T., Raymond, C. A., Sep. 2016. Cratering on Ceres: Implications for its crust and evolution. Science 353, aaf4758.

King, T. V. V., Clark, R. N., Calvin, W. M., Sherman, D. M., Brown, R. H., 1992. Evidence for ammonium-bearing minerals on Ceres. Science 255, 1551–1553. DOI: 10.1126/science.255.5051.1551.

Krohn, K., Jaumann, R., Stephan, K., Otto, K. A., Schmedemann, N., Wag- ner, R. J., Matz, K.-D., Tosi, F., Zambon, F., Gathen, I., Schulzeck, F., Schroeder, S. E., Buczkowski, D. L., Hiesinger, H., McSween, H. Y., Pieters, C. M., Preusker, F., Roatsch, T., Raymond, C. A., Russell, C. T., Williams, D. A., Dec. 2016. Cryogenic flow features on Ceres: Implications for crater-related cryovolcanism. 43, 11.

Larson, H. P., Feierberg, M. A., Fink, U., Smith, H. A., 1979. Remote spectroscopic identification of carbonaceous chondrite mineralogies Applications to Ceres and Pallas. Icarus 39, 257–271. DOI: 10.1016/0019– 1035(79)90168–4.

Lebofsky, L. A., 1978. Asteroid 1 Ceres - Evidence for water of hydration. Monthly Notices of the Royal Astronomical Society 182, 17P–21P. DOI: 10.1093/mnras/182.1.17P.

Lebofsky, L. A., Feierberg, M. A., Tokunaga, A., Larson, H. P., Johnson, J., 1981. The 1.7- to 4.2-micron spectrum of asteroid 1 Ceres - Evidence for structural water in clay minerals. Icarus 48, 453–459. DOI: 10.1016/0019– 1035(81)90055–5.

Li, J.-Y., Reddy, V., Nathues, A., Le Corre, L., Izawa, M. R. M., Cloutis, E. A., Sykes, M. V., Carsenty, U., Castillo-Rogez, J. C., Hoffmann, M., Jaumann, R., Krohn, K., Mottola, S., Prettyman, T. H., Schaefer, M., Schenk, P., Schr¨oder, S. E., Williams, D. A., Smith, D. E., Zuber, M. T., Konopliv, A. S., Park, R. S., Raymond, C. A., Russell, C. T., Feb. 2016. Surface Albedo and Spectral Variability of Ceres. 817, L22.

Longobardo, A., et. al., 2017. Mineralogy of the Occator Quadrangle. Icarus this issue.

Milliken, R. E., Rivkin, A. S., 2009. Brucite and carbonate assemblages from altered olivine-rich materials on Ceres. Nature Geoscience 2 (4), 258–261. DOI: 10.1038/ngeo478.

Nathues, A., Hoffmann, M., Platz, T., Thangjam, G. S., Cloutis, E. A., Reddy, V., Le Corre, L., Li, J.-Y., Mengel, K., Rivkin, A., Applin, D. M., Schaefer, M., Christensen, U., Sierks, H., Ripken, J., Schmidt, B. E., Hiesinger, H., Sykes, M. V., Sizemore, H. G., Preusker, F., Russell, C. T., Dec. 2016. FC colour images of dwarf planet Ceres reveal a complicated geological history. 134, 122–127.

Nathues, A., Hoffmann, M., Schaefer, M., Le Corre, L., Reddy, V., Platz, T., Cloutis, E. A., Christensen, U., Kneissl, T., Li, J.-Y., Mengel, K., Schmedemann, N., Schaefer, T., Russell, C. T., Applin, D. M., Buczkowski, D. L., Izawa, M. R. M., Keller, H. U., O'Brien, D. P., Pieters, C. M., Raymond, C. A., Ripken, J., Schenk, P. M., Schmidt, B. E., Sierks, H., Sykes, M. V., Thangjam, G. S., Vincent, J.-B., Dec. 2015. Sublimation in bright spots on (1) Ceres. Nature 528, 237–240.

Nettles, J. W., Staid, M., Besse, S., Boardman, J., Clark, R. N., Dhingra, D., Isaacson, P., Klima, R., Kramer, G., Pieters, C. M., Taylor, L. A., Jul. 2011. Optical maturity variation in lunar spectra as measured by Moon Mineralogy Mapper data. Journal of Geophysical Research (Planets) 116, E00G17.

Palomba, E., et. al., 2017. Submitted. Compositional differences among Bright Spots on the Ceres surface. Icarus.

Pasckert, J. H., et. al., 2017. Icarus. The Geological Mapping on Ceres.

Pieters, C. M., Staid, M. I., Fischer, E. M., Tompkins, S., He, G., Dec. 1994. A Sharper View of Impact Craters from Clementine Data. Science 266, 1844–1848.

Platz, T., Nathues, A., Sizemore, H. G., Crown, D. A., Hoffmann, M., Scha ̈fer, M., Schmedemann, N., Kneissl, T., Neesemann, A., Mest, S. C., Buczkowski, D. L., Ruesch, O., Naß, A., Williams, D. A., Preusker, F., Mar. 2017. Geological Mapping of the Ac-10 Rongo Quadrangle of Ceres. In: Lunar and Planetary Science Conference. Vol. 48 of Lunar and Plane- tary Science Conference. p. 2551.

Prettyman, T. H., Feldman, W. C., McSween, H. Y., Dingler, R. D., Ene- mark, D. C., Patrick, D. E., Storms, S. A., Hendricks, J. S., Morgenthaler, J. P., Pitman, K. M., Reedy, R. C., 2011. Dawn's Gamma Ray and Neutron Detector. Space Science Reviews 163, 371–459. DOI: 10.1007/s11214–011–9862–0.

Preusker, F., Scholten, F., Matz, K.-D., Elgner, S., Jaumann, R., Roatsch, T., Joy, S.P., Polanskey, C.A., Raymond, C.A., Russell, C.T., 2016. 47th Lunar and Planetary Science Conference, The Woodlands, Texas, 21-25 March 2016. LPI Contribution No. 1903, p.1954. ADS Bibcode: 2016LPI....47.1954P.

Raponi, A., 2017. This issue. Mineralogical mapping of Coniraya Quadrangle of the Dwarf Planet Ceres. Icarus.

Raymond, C.A., Roatsch, T., 2015. Ceres coordinate system description. https://sbn.psi.edu/pds/resource/ceres_coord_sys_151014.pdf

Rivkin, A. S., Volquardsen, E. L., Clark, R. N., 2006. The surface composi- tion of Ceres: Discovery of carbonates and iron-rich clays. Icarus 185 (2), 563–567. DOI: 10.1016/j.icarus.2006.08.022.

Roatsch, T., Kersten, E., Matz, K.-D., Preusker, F., Scholten, F., Jaumann, R., Raymond, C. A., Russell, C. T., Sep. 2016. High-resolution Ceres High Altitude Mapping Orbit atlas derived from Dawn Framing Camera images. 129, 103–107.

Ruesch, O., Platz, T., Schenk, P. M., McFadden, L., Castillo-Rogez, J., Quick, L. C., Byrne, S., O'Brien, D. P., Schmedemann, N., Williams, D. A., Li, J.-Y., Bland, P. A., Hiesinger, H., Kneissl, T., Neesemann, A., Schaefer, M., Pasckert, J. H., Schmidt, B. E., Buczkowski, D. L., Sykes, M. V., Nathues, A., Roatsch, T., Hoffmann, M., Raymond, C. A., Russell, C. T., 2016. Cryovolcanic on Ceres. Science 353 (6303), DOI: 10.1126/science.aaf4286.

Russell, C. T., Raymond, C. A., Ammannito, E., Buczkowski, D. L., De Sanctis, M. C., Hiesinger, H., Jaumann, R., Konopliv, A. S., McSween, H. Y., Nathues, A., Park, R. S., Pieters, C. M., Prettyman, T. H., McCord, T. B., McFadden, L. A., Mottola, S., Zuber, M. T., Joy, S. P., Polanskey, C., Rayman, M. D., Castillo-Rogez, J. C., Chi, P. J., Combe, J. P., Er- makov, A., Fu, R. R., Hoffmann, M., Jia, Y. D., King, S. D., Lawrence, D. J., Li, J.-Y., Marchi, S., Preusker, F., Roatsch, T., Ruesch, O., Schenk, P., Villarreal, M. N., Yamashita, N., Sep. 2016. Dawn arrives at Ceres: Exploration of a small, volatile-rich world. Science 353, 1008–1010.

Schmedemann, N., Kneissl, T., Neesemann, A., Stephan, K., Jaumann, R., Krohn, K., Michael, G. G., Matz, K. D., Otto, K. A., Raymond, C. A., Russell, C. T., Dec. 2016. Timing of optical maturation of recently exposed material on Ceres. 43, 11.

Schro¨der, S. E., Mottola, S., Carsenty, U., Ciarniello, M., Jaumann, R., Li, J.-Y., Longobardo, A., Palmer, E., Pieters, C., Preusker, F., Raymond, C. A., Russell, C. T., May 2017. Resolved spectrophotometric properties of the Ceres surface from Dawn Framing Camera images. 288, 201–225.

Sierks, H., Keller, H. U., Jaumann, R., Michalik, H., Behnke, T., Bubenhagen, F., Buttner, I., Carsenty, U., Christensen, U., Enge, R., Fiethe, B., Gutierrez Marques, P., Hartwig, H., Kruger, H., Kuhne, W., Maue, T., Mottola, S., Nathues, A., Reiche, K.-U., Richards, M. L., Roatsch, T., Schroder, S. E., Szemerey, I., Tschentscher, M., 2011. The Dawn Framing Camera. Space Science Reviews 163, 263–327.

Singh, S., et. al., 2017. Mineralogy Mapping of the Ac-H-5 Fejokoo quadran- gle of Ceres. Icarus, this issue.

Stephan, K., Jaumann, R., Krohn, K., Schmedemann, N., Zambon, F., Tosi, F., Carrozzo, F. G., McFadden, L. A., Otto, K., De Sanctis, M. C., Ammannito, E., Matz, K.-D., Roatsch, T., Preusker, F., Raymond, C. A., Russell, C. T., Feb. 2017. An investigation of the bluish material on Ceres. 44, 1660–1668.

Tosi, F., et. al., 2017. Mineralogical Analysis of the Haulani Quadrangle of the Dwarf Planet Ceres. Icarus, this issue.

Tosi, F., Frigeri, A., Combe, J.-P., Zambon, F., De Sanctis, M. C., Ammannito, E., Longobardo, A., Hoffman, M., Nathues, A., Garry, W., Blewett, D. T., Pieters, C. M., Palomba, E., Stephan, K., McFadden, L. A., Mc- Sween, H. Y., Russell, C. T., Raymond, C. A., the Dawn Science Team, 2015. Mineralogical analysis of the Oppia quadrangle of asteroid (4) Vesta: Evidence for occurrence of moderate-reflectance hydrated minerals. Icarus 259, 129–149. DOI: 10.1016/j.icarus.2015.05.018.

Williams, D. A., et. al., 2017. Icarus. The Geological Mapping on Ceres.

Zambon, F., Frigeri, A., Combe, J.-P., Tosi, F., Longobardo, A., Ammannito, E., De Sanctis, M. C., Blewett, D. T., Scully, J. E. C., Palomba, E., Denevi, B. W., Yingst, A., Russell, C. T., Raymond, C. A., 2015. Spectral Analysis of the Quadrangles Av-13 and Av-14 on Vesta. Icarus 259, 181–193. DOI: 10.1016/j.icarus.2015.05.015.

Zambon, F., Raponi, A., Tosi, F., De Sanctis, M. C., McFadden, L. A., Carrozzo, F. G., Longobardo, A., Ciarniello, M., Krohn, K., Stephan, K., Palomba, E., Pieters, C. M., Ammannito, E., Russell, C. T., Raymond, C. A., Jan. 2017. Spectral analysis of Ahuna Mons from Dawn mission's visible-infrared spectrometer. 44, 97–104.

Zambon, F., Tosi, F., Carli, C., De Sanctis, M. C., Blewett, D. T., Palomba, E., Longobardo, A., Frigeri, A., Ammannito, E., Russell, C. T., Raymond, C. A., Jul. 2016. Lithologic variation within bright material on Vesta revealed by linear spectral unmixing. 272, 16–31.

Figures

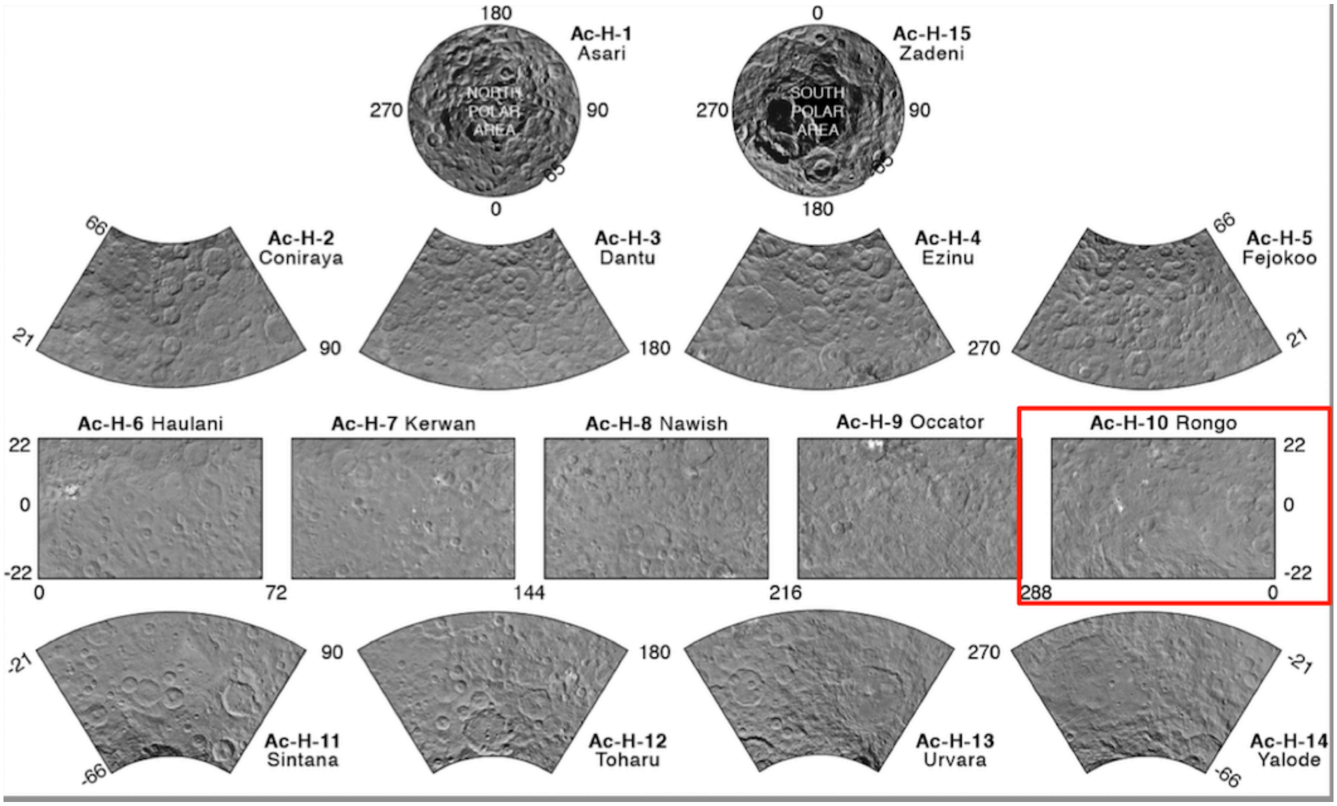

Figure 1

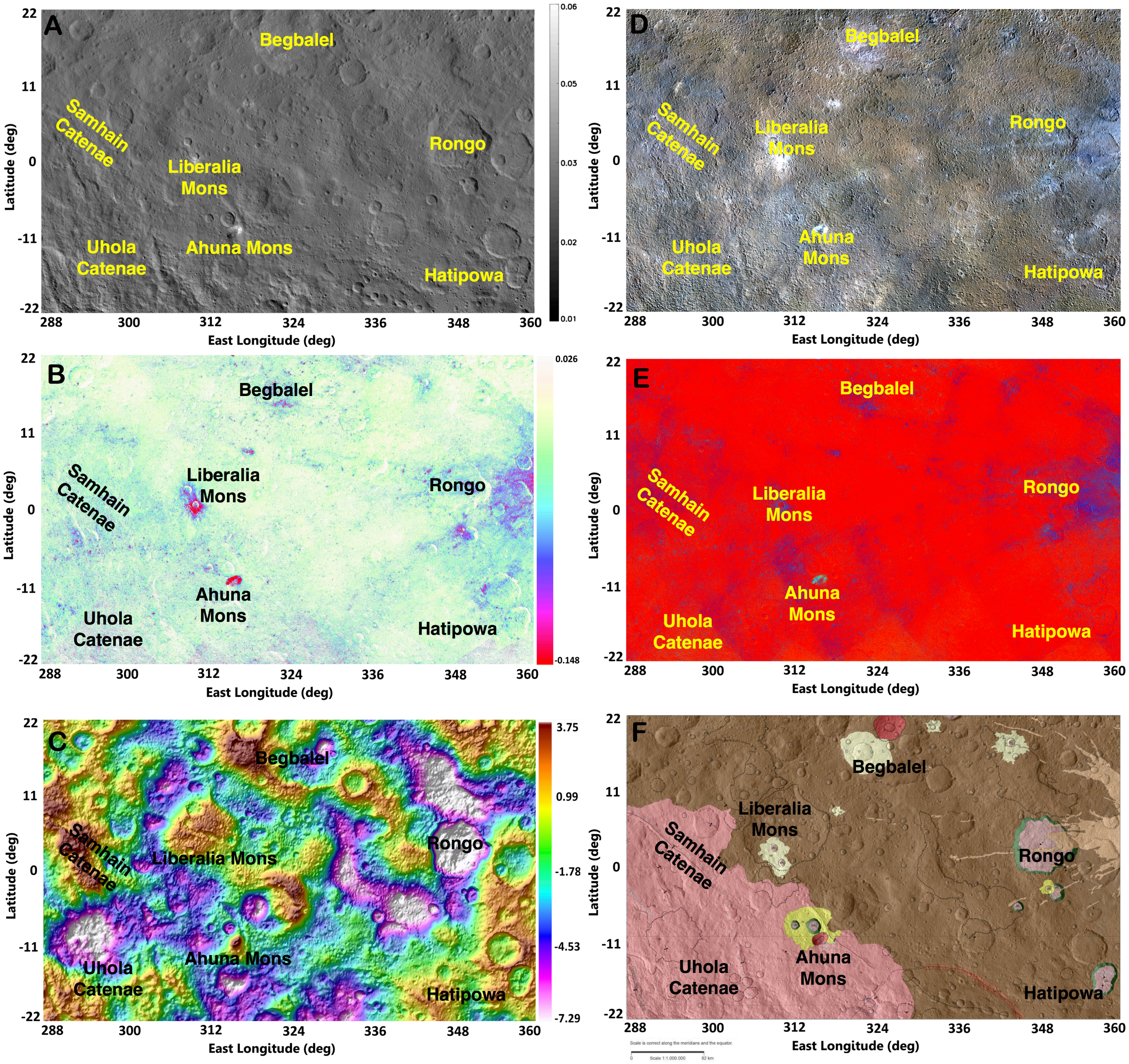
A
Begbalel
Samhain Catenae
Liberalia Mons
Rongo
Uhola Catenae
Ahuna Mons
Hatipowa
0.06
0.05
0.03
0.02
0.01
B
Begbalel
Samhain Catenae
Liberalia Mons
Rongo
Ahuna Mons
Uhola Catenae
Hatipowa
0.026
-0.148
C
Begbalel
Samhain Catenae
Liberalia Mons
Rongo
Ahuna Mons
Uhola Catenae
Hatipowa
3.75
0.99
-1.78
-4.53
-7.29
D
Begbalel
Samhain Catenae
Liberalia Mons
Rongo
Uhola Catenae
Ahuna Mons
Hatipowa
E
Begbalel
Samhain Catenae
Liberalia Mons
Rongo
Ahuna Mons
Uhola Catenae
Hatipowa
F
Begbalel
Liberalia Mons
Samhain Catenae
Rongo
Ahuna Mons
Uhola Catenae
Hatipowa
Latitude (deg)
22
11
0
-11
-22
East Longitude (deg)
288
300
312
324
336
348
360
Scale is correct along the meridians and the equator.
0
Scale 1:1.000.000
82 km

Figure 2

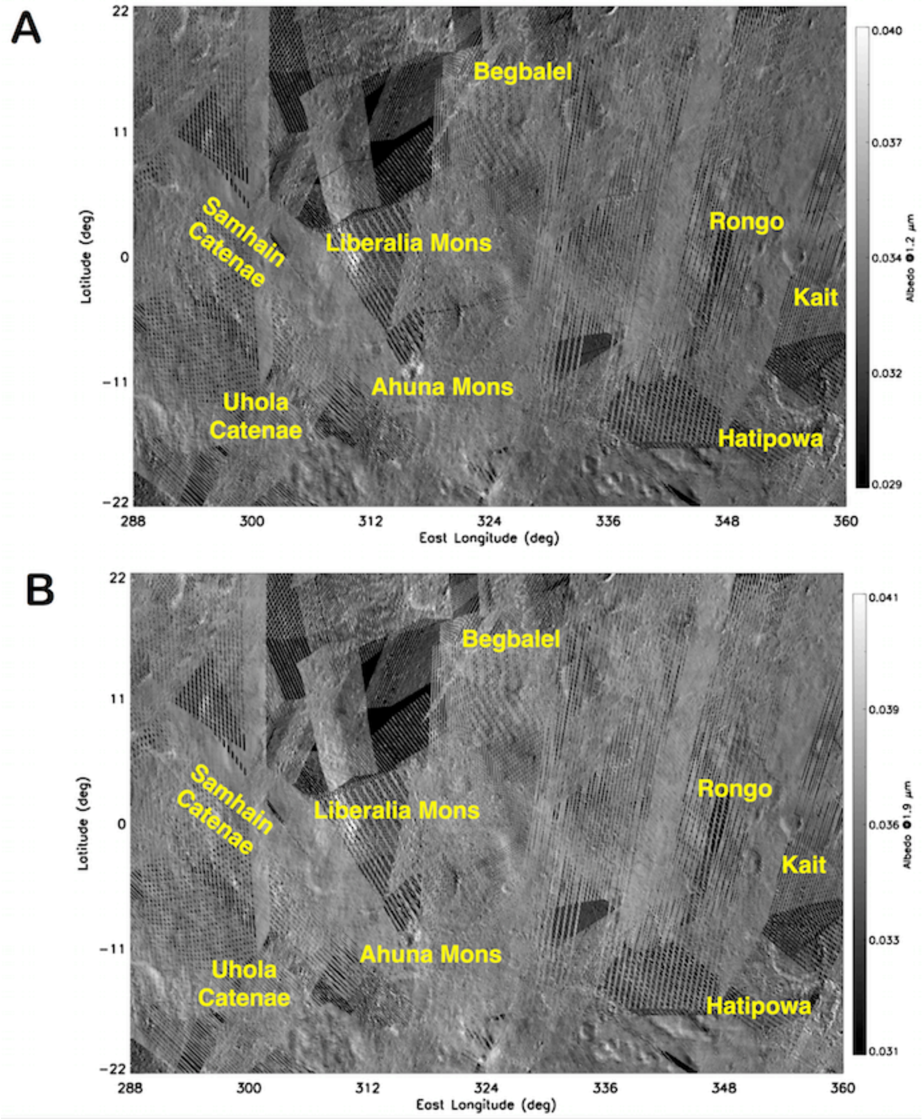
A
B
Begbalel
Samhain Catenae
Liberalia Mons
Rongo
Kait
Uhola Catenae
Ahuna Mons
Hatipowa
Latitude (deg)
22
11
0
−11
−22
288
300
312
324
336
348
360
East Longitude (deg)
Albedo @1.2 μm
0.040
0.037
0.034
0.032
0.029
Albedo @1.9 μm
0.041
0.039
0.036
0.033
0.031

Figure 3

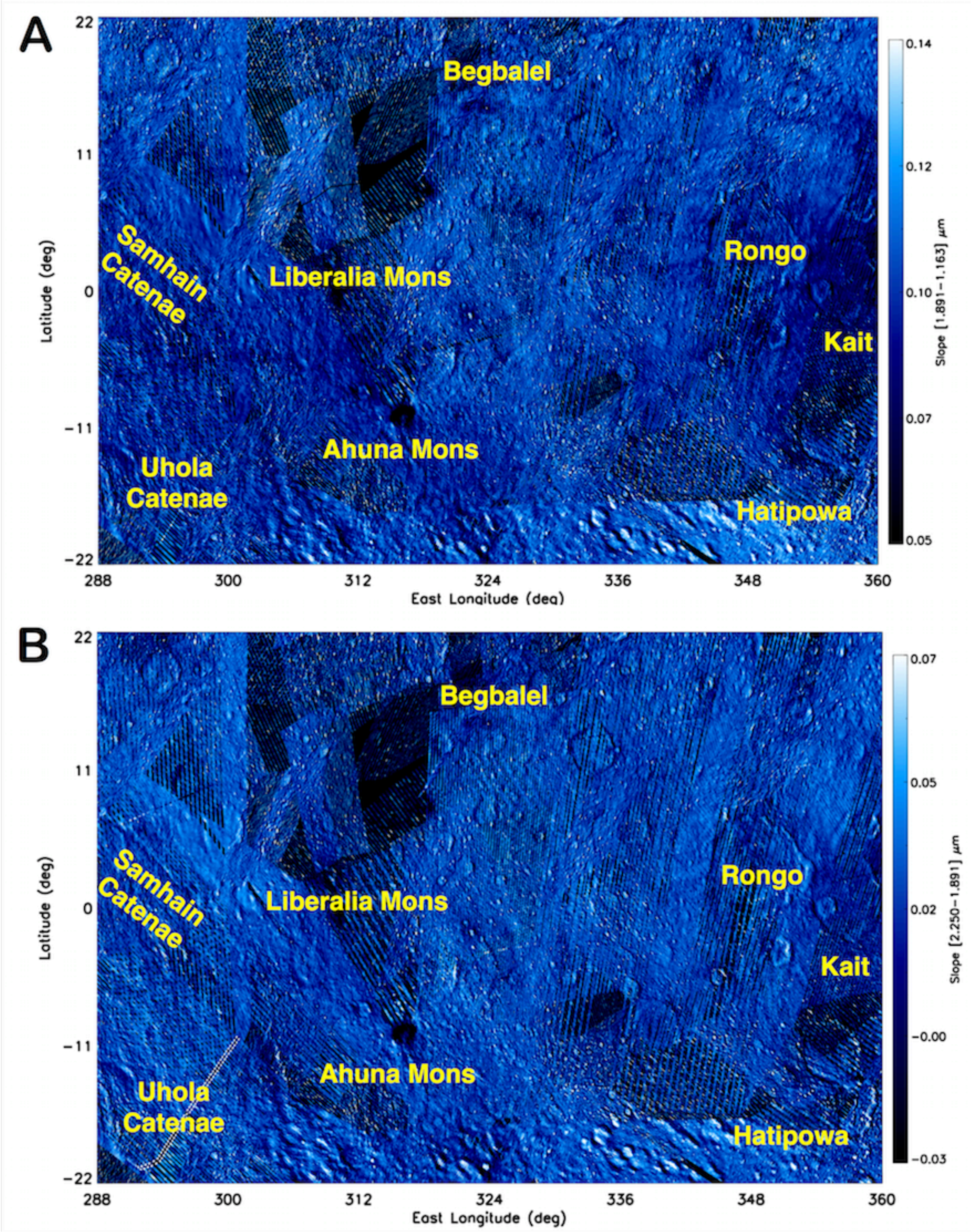
A
B
Begbalel
Samhain Catenae
Liberalia Mons
Rongo
Kait
Ahuna Mons
Uhola Catenae
Hatipowa
Latitude (deg)
East Longitude (deg)
22
11
0
−11
−22
288
300
312
324
336
348
360
Slope [1.891−1.163] µm
0.14
0.12
0.10
0.07
0.05
Slope [2.250−1.891] µm
0.07
0.05
0.02
−0.00
−0.03

Figure 4

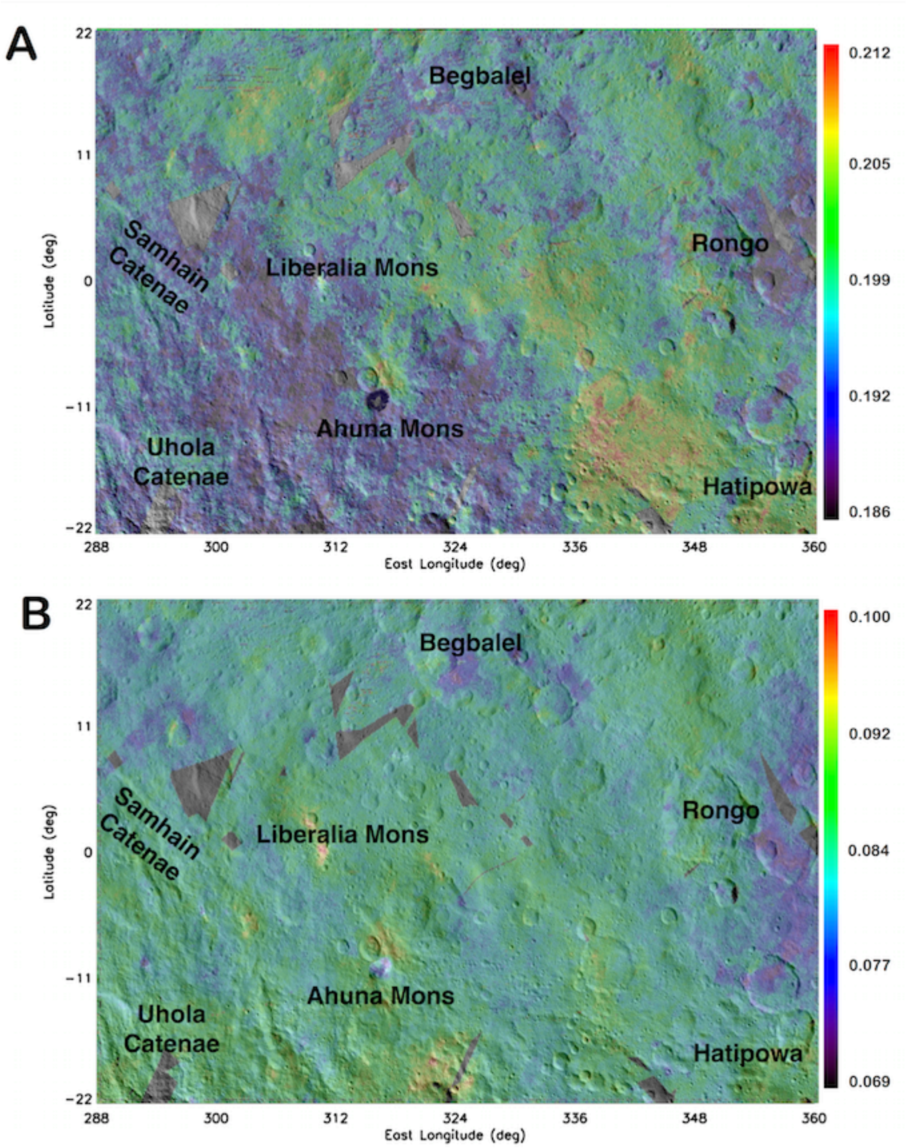
A
Begbalel
Rongo
Samhain Catenae
Liberalia Mons
Ahuna Mons
Uhola Catenae
Hatipowa
Latitude (deg)
22
11
0
−11
−22
288
300
312
324
336
348
360
East Longitude (deg)
0.212
0.205
0.199
0.192
0.186
B
Begbalel
Rongo
Samhain Catenae
Liberalia Mons
Ahuna Mons
Uhola Catenae
Hatipowa
Latitude (deg)
22
11
0
−11
−22
288
300
312
324
336
348
360
East Longitude (deg)
0.100
0.092
0.084
0.077
0.069

Figure 5

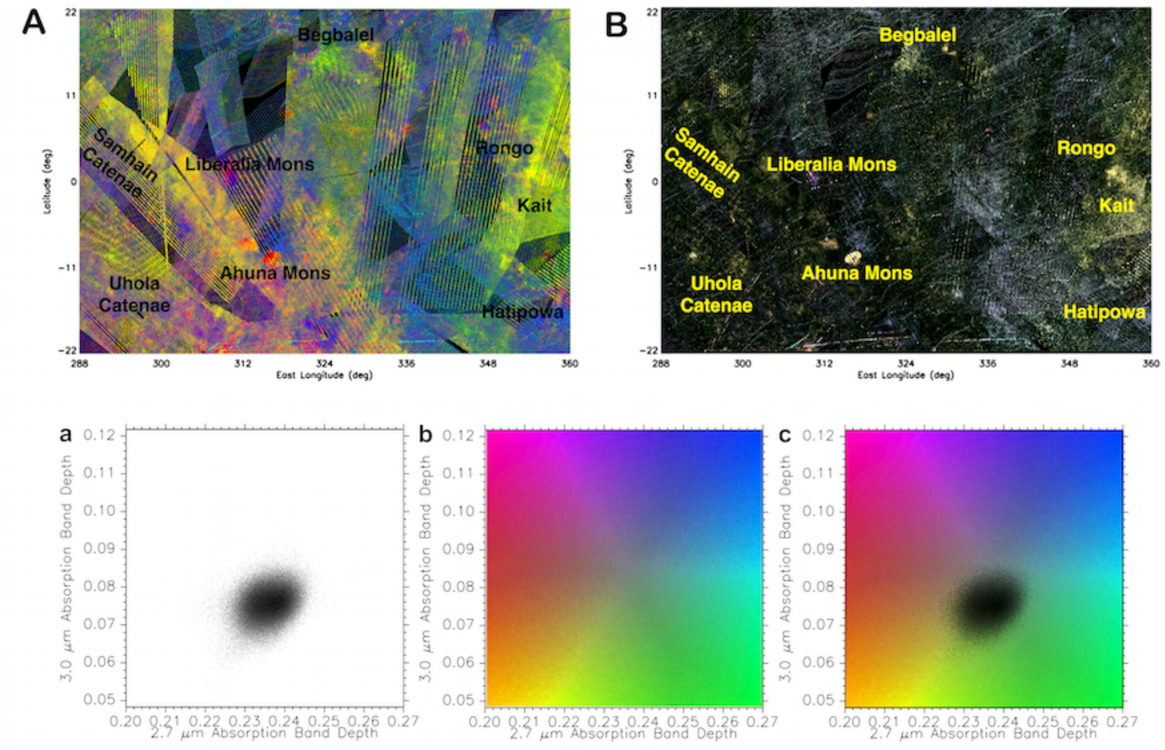
A
B
Begbalel
Samhain Catenae
Liberalia Mons
Rongo
Kait
Uhola Catenae
Ahuna Mons
Hatipowa
Latitude (deg)
22
11
0
-11
-22
East Longitude (deg)
288
300
312
324
336
348
360
a
b
c
3.0 µm Absorption Band Depth
0.12
0.11
0.10
0.09
0.08
0.07
0.06
0.05
2.7 µm Absorption Band Depth
0.20
0.21
0.22
0.23
0.24
0.25
0.26
0.27

Figure 6

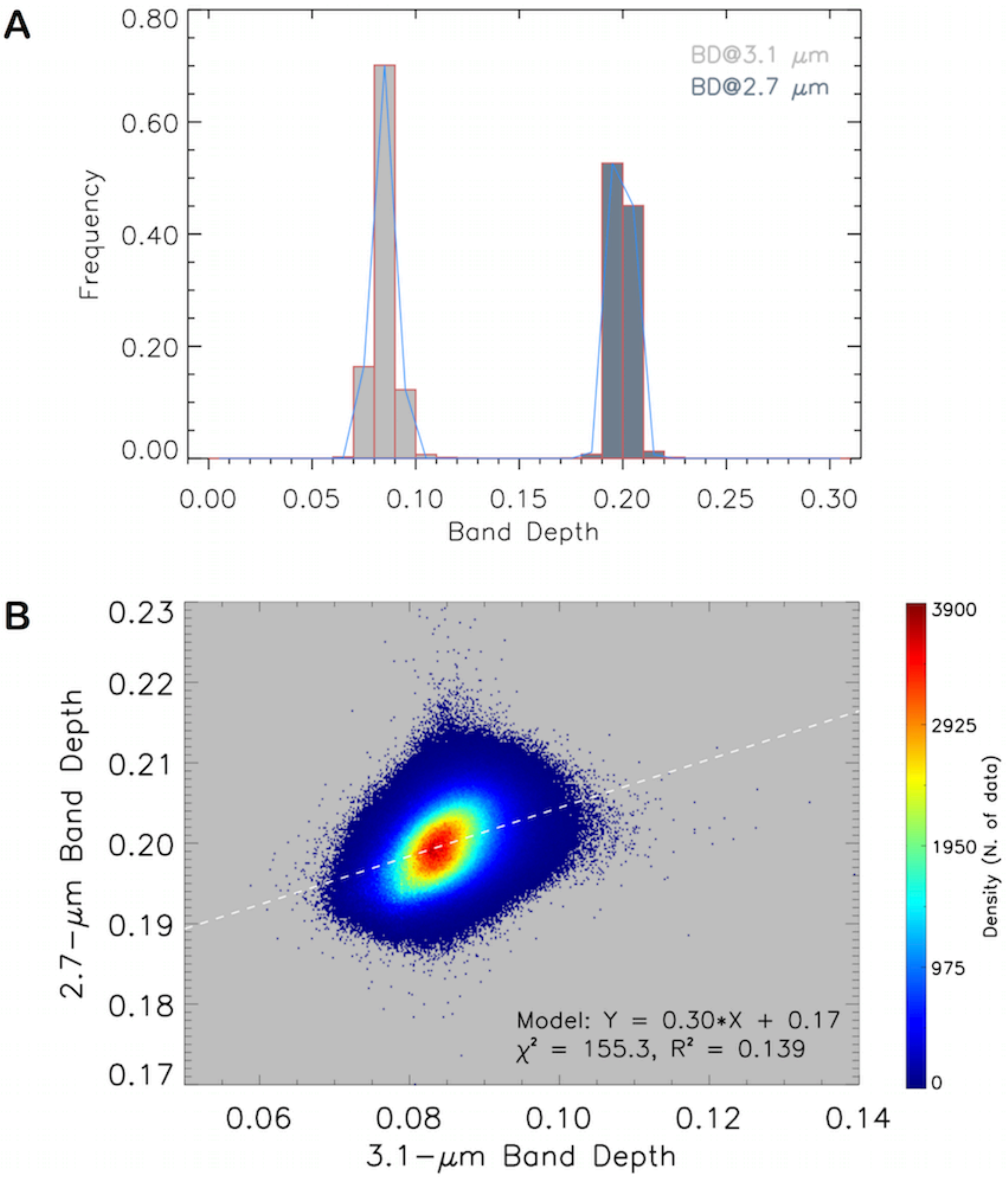
A
BD@3.1 μm
BD@2.7 μm
Frequency
0.00
0.20
0.40
0.60
0.80
Band Depth
0.00
0.05
0.10
0.15
0.20
0.25
0.30
B
2.7−μm Band Depth
0.17
0.18
0.19
0.20
0.21
0.22
0.23
3.1−μm Band Depth
0.06
0.08
0.10
0.12
0.14
Model: Y = 0.30*X + 0.17
χ² = 155.3, R² = 0.139
Density (N. of data)
0
975
1950
2925
3900

Figure 7

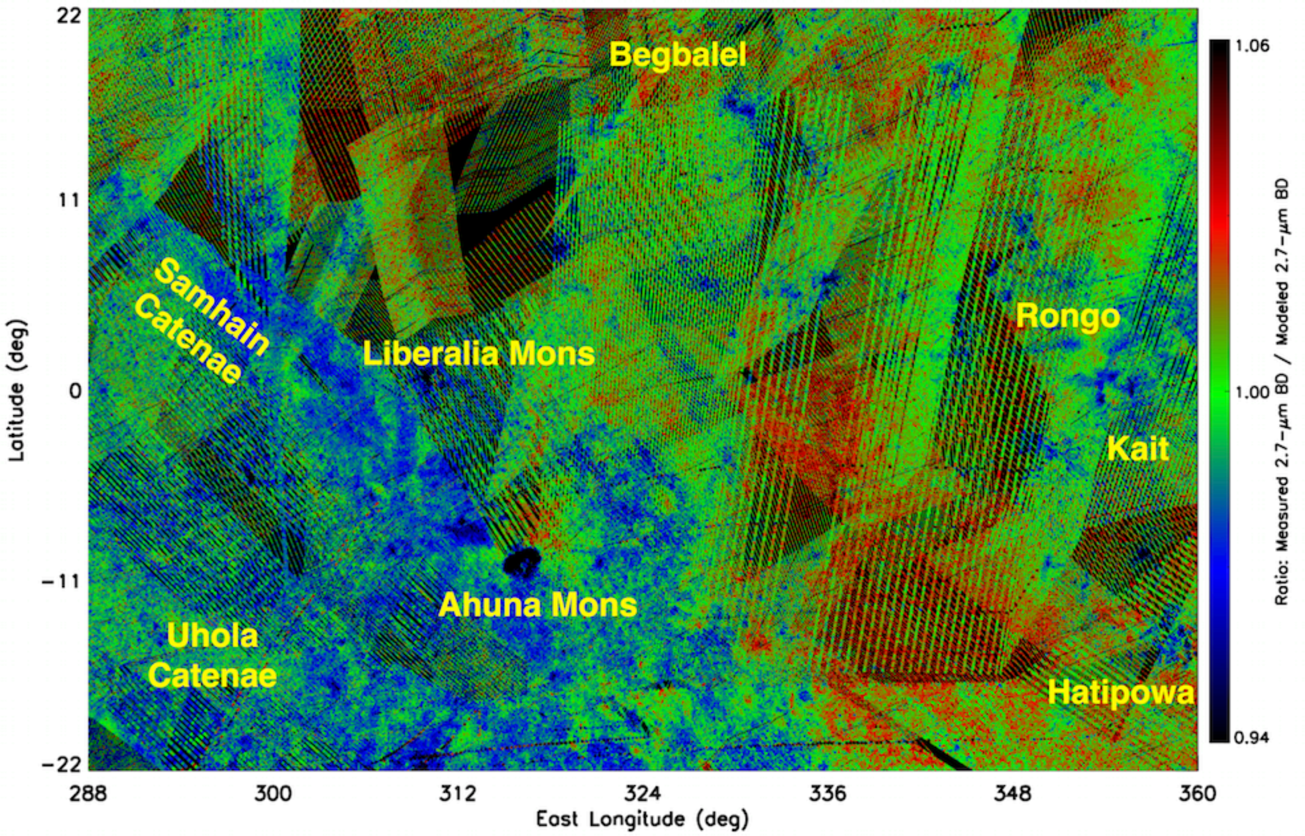
22
11
0
−11
−22
Latitude (deg)
288
300
312
324
336
348
360
East Longitude (deg)
Begbalel
Samhain Catenae
Liberalia Mons
Rongo
Kait
Ahuna Mons
Uhola Catenae
Hatipowa
1.06
1.00
0.94
Ratio: Measured 2.7−μm BD / Modeled 2.7−μm BD

Figure 8